PERGAMON

International Journal of Heat and Mass Transfer 45 (2002) 2277–2287

International Journal of HEAT and MASS TRANSFER

www.elsevier.com/locate/ijhmt

A two-phase flow and transport model for the cathode of PEM fuel cells

Lixin You [a], Hongtan Liu [b,*]

[a] *Dais-Analytic Corporation, 100 Cummings Park, Woburn, MA 01801, USA*

[b] *Department of Mechanical Engineering, University of Miami, P.O. Box 248294, Coral Gables, FL 33124-0624, USA*

Received 26 January 2001; received in revised form 18 October 2001

Abstract

A unified two-phase flow mixture model has been developed to describe the flow and transport in the cathode for PEM fuel cells. The boundary condition at the gas diffuser/catalyst layer interface couples the flow, transport, electrical potential and current density in the anode, cathode catalyst layer and membrane. Fuel cell performance predicted by this model is compared with experimental results and reasonable agreements are achieved. Typical two-phase flow distributions in the cathode gas diffuser and gas channel are presented. The main parameters influencing water transport across the membrane are also discussed. By studying the influences of water and thermal management on two-phase flow, it is found that two-phase flow characteristics in the cathode depend on the current density, operating temperature, and cathode and anode humidification temperatures.

Keywords: Two-phase flow; Porous electrode; Proton exchange membrane (PEM); Fuel cells; Mathematical model; Simulation; Water and thermal management

1. Introduction

A proton exchange membrane (PEM) fuel cell consists of an anode, a cathode and a hydrated polymer membrane as the electrolyte. The use of a solid membrane reduces corrosion and electrolyte management problems. Thus, PEM fuel cells may operate at a low temperature. They also have high power density, short response time and quick startup capability. In addition, virtually no pollutant is produced during this fuel cell operation. Therefore, the PEM fuel cell system is considered to be one of the most promising future vehicular power systems. It also has a promising future with portable electronics, uninterrupted power system (UPS) and distributed power systems.

Water and thermal management is essential for proper operation of PEM fuel cells. The polymer membrane in the PEM fuel cell must be in a highly hydrated state to facilitate proton transport. If there is not enough water, the membrane becomes dehydrated and its resistance to proton conduction increases sharply. On the other hand, if too much water is present, flooding may occur resulting in the pores of the gas diffuser filled by liquid water, which will block the transport of reactants to the reaction sites. In practice, humidification of anode fuels and/or cathode oxidants is often used to provide sufficient membrane hydration. Since water is produced in the cathode catalyst layer and water also tends to migrate from the anode side to the cathode side under the electro-osmotic drag, it becomes a key issue to avoid flooding in the cathode in the design and operation of PEM fuel cells.

There have been some studies on water and thermal management as well as performance modeling for PEM fuel cells. Bernardi and Verbrugge [1,2] and Springer [3] proposed one-dimensional models that provided good preliminary foundations for PEM fuel cell modeling. However, a one-dimensional model cannot simulate the decrease of reactants and the accumulation of products in the flow direction. The two-dimensional models by Fuller and Newman [4] and Nguyen and White [5]

* Corresponding author. Tel.: +1-305-284-2019; fax: +1-305-284-2580.

E-mail address: hliu@miami.edu (H. Liu).

0017-9310/02/$ - see front matter
PII: S0017-9310(01)00322-2

Nomenclature

C	species mass fraction
d	width (m)
D	diffusion coefficient (m^2/s)
F	Faraday constant (96493 C/mol)
I	current density (A/cm^2)
j	diffusive mass flux (kg/m^2 s)
$J(s)$	capillary pressure function
k_r	relative permeability
K	absolute permeability (m^2)
l	fluid channel length (m)
M	molecular weight (kg/mol)
n	number of electrons or water transport coefficient in the membrane (number of water molecules transfer per proton)
N	molar flux (mol/cm^2 s)
P	pressure (Pa)
R	universal gas constant (J/mol K)
s	phase saturation
T	temperature (K)
u	velocity vector (m/s)
u	the x-direction velocity component (m/s)
v	y-direction velocity component (m/s)

Greek symbols

α	net water transport coefficient
ε	porosity
γ	multiphase correction factor
η	potential difference from equilibrium (overpotential) (V)
λ	water content in membrane (mol H_2O/equivalent SO_3^{-1}) or individual mobility
μ	dynamic viscosity (N s/m^2)
ν	kinematic viscosity (m^2/s)
ρ	density (kg/cm^3)
σ	interfacial tension (N/m)

Subscripts and superscripts

c	capillary
d	porous media or electro-osmotic drag
diff	diffusion
eff	effective property that accounts for porosity, tortuosity and liquid water
g	gas phase
hyd	hydraulic permeation
k	phase k
l	liquid phase
m	membrane
r	relative
v	vapor
w	wet or water
α	species

assumed that diffusion was the only mechanism for oxygen transport and did not consider the interaction of the flow with the species field in the channel and gas diffuser. By using computational fluid dynamics (CFD), Gurau and Liu [6] presented the first unified approach by coupling the flow and transport governing equations in the flow channel and the gas diffuser, but only a single-phase incompressible model was used. Wang et al. [7] classified four regimes of water transport and distribution in the PEMFC air cathode and presented some interesting two-phase flow and transport results, but their model did not include the catalyst layer, the membrane and the anode side.

In this paper, a two-phase flow model based on a "multiple-phase mixture" concept is developed to examine the flow field in the coupled domain of cathode gas diffuser and the gas channel. Wang and Cheng [8] first proposed a detailed multiphase mixture mathematical model for multiphase flow in the porous media. The key idea in the multiphase mixture model is to focus on the level of a multiphase mixture, rather than on the levels of separate phases. The multiple phases are regarded as constituents of a multiphase mixture in the model, so that a multiphase flow can be described by a mass-averaged mixture velocity and a diffusive flux representing the differences between the mixture velocity and individual phase velocities. In this definition, phases are assumed to be distinct and separable components with nonzero interfacial areas, and their mixture represents a single fluid with smoothly varying phase composition. The multiphase mixture model can be derived from the classical multiphase approach without any additional assumptions; see [8,9] for details.

2. Mathematical model

2.1. Two-phase flow and multi-component species governing equations

The modeling domain of the PEM fuel cell cathode is shown in Fig. 1. The area ABCD is the fluid channel and the area CDEF is the porous electrode (including the gas diffuser and the catalyst layer). The humidified air flows into the domain along the channel at a velocity u_{in}, and flows out the domain from the right channel boundary BC.

Reacting with protons transferred through membrane and electrons from outer circuit, oxygen is reduced to water in the catalyst layer. Water may also transport from the anode to the cathode side under the combined actions of the electro-osmotic drag and back

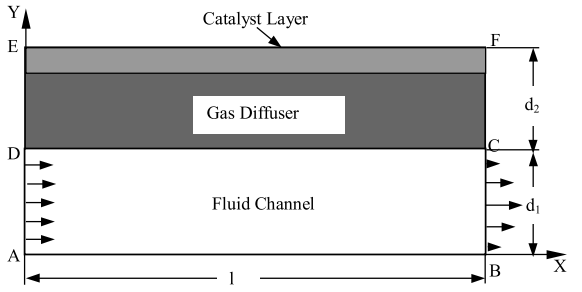

Fig. 1. The fluid channel and porous medium coupled domain.

diffusion and hydraulic permeation in the membrane. When the partial pressure of water vapor exceeds the saturated vapor pressure, liquid water is formed, and there will be two-phase flow in the PEM fuel cell. Liquid water may block the pores of the gas diffuser, which are essential for oxygen diffusion. Predicting the formation of liquid water and minimizing its detrimental effect on fuel cell performance are important issues in the design and operation of PEM fuel cells. A single-phase flow model is obviously not capable of describing two-phase phenomena, thus a two-phase flow model is necessary to understand the transport phenomena.

The following assumptions are used in the model development:

1. The flow is laminar everywhere.
2. Only steady state is considered.
3. The gas diffusers, catalyst layers and membrane are considered as isotropic porous media.
4. The domain is isothermal.

As shown in Fig. 1, the humidified air flows in a heterogeneous domain that includes a homogeneous fluid and a porous medium. If the governing equations are written separately in the fluid channel and gas diffuser, the boundary conditions at the gas channel/gas diffuser interface are difficult to specify, and a considerable effort is needed to couple the flow and transport of both regions. Since the velocity, pressure and species mass fractions are continuous at the gas channel/gas diffuser interface, a unified approach is applicable [6]. The unified approach solves the governing equations in the gas channel and gas diffuser simultaneously, so the necessity to specify the interface boundary conditions is avoided.

At any location in the gas diffuser and the gas channel, the total mass of the two-phase mixture is conserved

$$\varepsilon\frac{\partial\rho}{\partial t}+\nabla\cdot(\rho\mathbf{u})=0. \tag{1}$$

For the two-phase mixture in the gas channel, the Navier–Stokes equation is applicable

$$\frac{\partial(\rho\mathbf{u})}{\partial t}+\nabla\cdot(\rho\mathbf{u}\mathbf{u})=-\nabla P+\nabla\cdot(\nabla\mu\mathbf{u}). \tag{2}$$

Darcy's law is usually used to describe the momentum conservation in a porous medium (for example, [8]). However, since the gas diffuser is very thin and the velocity gradient is very high at its interface with the gas channel, the macroscopic inertial force and viscous force cannot be neglected. A generalized Darcy law [10] is more suitable for describing the two-phase mixture flow in the gas diffuser

$$\frac{\partial(\rho\mathbf{u})}{\partial t}+\nabla\cdot(\rho\mathbf{u}\mathbf{u})=-\nabla P+\nabla\cdot(\nabla\mu\mathbf{u})-\frac{\mu}{K}(\varepsilon\mathbf{u}). \tag{3}$$

Note that the interfacial shear force and surface tension gradient force between the liquid phase and the gas phase cancelled out and do not appear in Eqs. (2) and (3). It is obvious that Eq. (3) is similar to Eq. (2), which makes it possible to treat Eq. (2) as a special form of the general equation (3) and solve it in the coupled domain.

The species conservation equation for the two-phase mixture is given as [8]

$$\begin{aligned}&\varepsilon\frac{\partial}{\partial t}(\rho C^{\alpha})+\nabla\cdot(\gamma_{\alpha}\rho\mathbf{u}C^{\alpha})\\&\quad=\nabla\cdot(\varepsilon\rho D\nabla C^{\alpha})+\nabla\cdot\left[\varepsilon\sum_{k}[\rho_k s_k D_k^{\alpha}(\nabla C_k^{\alpha}-\nabla C^{\alpha})]\right]\\&\qquad-\nabla\cdot\left[\sum_{k}C_k^{\alpha}\mathbf{j}_k\right].\end{aligned} \tag{4}$$

We are dealing with a two-phase flow problem, so $k=2$ (liquid and gas phases); α denotes species here that include oxygen, nitrogen and water. The mixture quantities in the above formulation are defined as

$$\rho=\rho_{\mathrm{l}}s_{\mathrm{l}}+\rho_{\mathrm{g}}s_{\mathrm{g}}, \tag{5}$$

$$\rho\mathbf{u}=\rho_{\mathrm{l}}\mathbf{u}_{\mathrm{l}}+\rho_{\mathrm{g}}\mathbf{u}_{\mathrm{g}}, \tag{6}$$

$$\rho C^{\alpha}=\rho_{\mathrm{l}}s_{\mathrm{l}}C_{\mathrm{l}}^{\alpha}+\rho_{\mathrm{g}}s_{\mathrm{g}}C_{\mathrm{g}}^{\alpha}, \tag{7}$$

$$\rho D^{\alpha}=\rho_{\mathrm{l}}s_{\mathrm{l}}D_{\mathrm{l}}^{\alpha}+\rho_{\mathrm{g}}s_{\mathrm{g}}D_{\mathrm{g}}^{\alpha}, \tag{8}$$

$$v=\frac{1}{(k_{\mathrm{rl}}/v_{\mathrm{l}})+(k_{\mathrm{rg}}/v_{\mathrm{g}})}. \tag{9}$$

The correction factor γ_{α} in Eq. (4) indicates that species α is advected on the mixture level by a modified velocity field $\gamma_{\alpha}\mathbf{u}$ rather than by the original mixture velocity field and is defined as

$$\gamma_{\alpha}=\frac{\rho\left[\lambda_{\mathrm{l}}C_{\mathrm{l}}^{\alpha}+\lambda_{\mathrm{g}}C_{\mathrm{g}}^{\alpha}\right]}{\rho_{\mathrm{l}}s_{\mathrm{l}}C_{\mathrm{l}}^{\alpha}+\rho_{\mathrm{g}}s_{\mathrm{g}}C_{\mathrm{g}}^{\alpha}}, \tag{10}$$

where the individual mobility $\lambda_{\mathrm{l}},\lambda_{\mathrm{g}}$ are

$$\lambda_{\mathrm{l}}=\frac{k_{\mathrm{rl}}/v_{\mathrm{l}}}{k_{\mathrm{rl}}/v_{\mathrm{l}}+k_{\mathrm{rg}}/v_{\mathrm{g}}}, \tag{11}$$

$$\lambda_{\mathrm{g}}=\frac{k_{\mathrm{rg}}/v_{\mathrm{g}}}{k_{\mathrm{rl}}/v_{\mathrm{l}}+k_{\mathrm{rg}}/v_{\mathrm{g}}}. \tag{12}$$

As in a traditional mixture theory, a diffusive mass flux of phase k within the two-phase mixture can be defined as

$$\mathbf{j}_k = \rho_k \mathbf{u}_k - \lambda_k \rho \mathbf{u}, \tag{13}$$

$$\mathbf{j}_\mathrm{l} + \mathbf{j}_\mathrm{g} = 0, \tag{14}$$

$\mathbf{j}_\mathrm{l}$ can be expressed as

$$\mathbf{j}_\mathrm{l} = K\frac{\lambda_\mathrm{l}}{\nu}(\nabla P - \nabla P_\mathrm{l}) = K\frac{\lambda_\mathrm{l}\lambda_\mathrm{g}}{\nu}\nabla P_\mathrm{c}. \tag{15}$$

Once $\mathbf{j}_\mathrm{l}, \mathbf{j}_\mathrm{g}$ are determined, the individual phase velocities can be obtained from the mixture flow field by the following algebraic relations:

$$\rho_\mathrm{g}\mathbf{u}_\mathrm{g} = \mathbf{j}_\mathrm{g} + \lambda_\mathrm{g}\rho\mathbf{u}, \tag{16}$$

$$\rho_\mathrm{l}\mathbf{u}_\mathrm{l} = -\mathbf{j}_\mathrm{g} + \lambda_\mathrm{l}\rho\mathbf{u}. \tag{17}$$

2.2. Constitutive relations

The phase relative permeability is defined as the ratio of the intrinsic permeability for the phase at a given saturation to the total intrinsic permeability of the porous medium. The relative permeabilities for the liquid and gas phases are represented by the following empirical correlation, respectively [11],

$$k_\mathrm{rl} = s_\mathrm{l}^3, \tag{18}$$

$$k_\mathrm{rg} = (1 - s_\mathrm{l})^3. \tag{19}$$

The capillary pressure is assumed to be a function of saturation; the general empirical model is

$$P_\mathrm{c} = P_\mathrm{g} - P_\mathrm{l} = \sigma\left(\frac{\varepsilon}{K}\right)^{1/2} J(s_\mathrm{l}), \tag{20}$$

where $J(s_\mathrm{l})$ is the Leverett function, given by [12],

$$J(s_\mathrm{l}) = 1.417(1 - s_\mathrm{l}) - 2.120(1 - s_\mathrm{l})^2 + 1.263(1 - s_\mathrm{l})^3, \tag{21}$$

$$\nabla P_\mathrm{c} = \sigma\left(\frac{\varepsilon}{K}\right)^{1/2} J'(s_\mathrm{l})\nabla s_\mathrm{l} + \left(\frac{\varepsilon}{K}\right)^{1/2} J(s_\mathrm{l})\left[\sum_\alpha \frac{\partial\sigma}{\partial C^\alpha}\nabla C^\alpha + \frac{\partial\sigma}{\partial T}\nabla T\right]. \tag{22}$$

2.3. The gas–liquid phase equilibrium and the species equation simplification

Assume oxygen and nitrogen cannot dissolve in liquid water due to their low solubilities, we have,

$$C_\mathrm{l}^{\mathrm{O}_2} = 0, \quad C_\mathrm{l}^{\mathrm{N}_2} = 0, \quad C_\mathrm{l}^{\mathrm{H_2O}} = 1. \tag{23}$$

The vapor condenses when the vapor partial pressure exceeds the corresponding saturation vapor pressure [3] at the local temperature

$$\log_{10} P_\mathrm{v} = -2.1794 + 0.02953T - 9.1837\times10^{-5}T^2 + 1.4454\times10^{-7}T^3. \tag{24}$$

The corresponding vapor density is

$$\rho_\mathrm{v}^{\mathrm{H_2O}} = \frac{P_\mathrm{v}M}{RT}. \tag{25}$$

The concentration of water vapor in the gas mixture

$$C_\mathrm{g}^{\mathrm{H_2O}} = \frac{\rho_\mathrm{v}^{\mathrm{H_2O}}}{\rho_\mathrm{g}}. \tag{26}$$

For oxygen,

$$\rho C^{\mathrm{O}_2} = \rho_\mathrm{g} s_\mathrm{g} C_\mathrm{g}^{\mathrm{O}_2}. \tag{27}$$

Substitute Eq. (27) into Eq. (4), we obtain

$$\varepsilon\frac{\partial}{\partial t}(\rho C^{\mathrm{O}_2}) + \nabla\cdot(\gamma_{\mathrm{O}_2}\rho\mathbf{u}C^{\mathrm{O}_2}) = \nabla\cdot(\varepsilon\rho D_\mathrm{g}^{\mathrm{O}_2}\nabla C^{\mathrm{O}_2}) - \nabla\cdot\left(\frac{\rho}{\rho_\mathrm{g}s_\mathrm{g}}C^{\mathrm{O}_2}\mathbf{j}_\mathrm{g}\right). \tag{28}$$

Similarly, for nitrogen, we get

$$\varepsilon\frac{\partial}{\partial t}(\rho C^{\mathrm{N}_2}) + \nabla\cdot(\gamma_{N_2}\rho\mathbf{u}C^{\mathrm{N}_2}) = \nabla\cdot(\varepsilon\rho D_\mathrm{g}^{\mathrm{N}_2}\nabla C^{\mathrm{N}_2}) - \nabla\cdot\left(\frac{\rho}{\rho_\mathrm{g}s_\mathrm{g}}C^{\mathrm{N}_2}\mathbf{j}_\mathrm{g}\right) \tag{29}$$

and for water

$$\rho C^{\mathrm{H_2O}} = \rho_\mathrm{g} s_\mathrm{g} C_\mathrm{g}^{\mathrm{H_2O}} + \rho_\mathrm{l} s_\mathrm{l}. \tag{30}$$

Substitute Eq. (30) into Eq. (4), we obtain

$$\varepsilon\frac{\partial}{\partial t}(\rho C^{\mathrm{H_2O}}) + \nabla\cdot(\gamma_{\mathrm{H_2O}}\rho\mathbf{u}C^{\mathrm{H_2O}}) = \nabla\cdot(\varepsilon\rho D_\mathrm{g}^{\mathrm{H_2O}}\nabla C^{\mathrm{H_2O}}) - \nabla\cdot[\varepsilon\rho_\mathrm{l}D_\mathrm{g}^{\mathrm{H_2O}}\nabla s_\mathrm{l}] - \nabla\cdot\left[\left(\frac{\rho_\mathrm{v}^{\mathrm{H_2O}}}{\rho_\mathrm{g}} - 1\right)\mathbf{j}_\mathrm{g}\right]. \tag{31}$$

The gas mixture density is

$$\rho_\mathrm{g} = \frac{PM_\mathrm{g}}{RT}. \tag{32}$$

The two-phase mixture density is

$$\rho = \rho_\mathrm{g} s_\mathrm{g} + \rho_\mathrm{l} s_\mathrm{l}. \tag{33}$$

where, the liquid and gas phase saturations denote the volumetric fraction of the void space occupied by individual phases and are given, respectively, as

$$s_\mathrm{l} = \frac{\rho C^{\mathrm{H_2O}} - \rho_\mathrm{g} C_\mathrm{g}^{\mathrm{H_2O}}}{\rho_\mathrm{l} - \rho_\mathrm{g} C_\mathrm{g}^{\mathrm{H_2O}}}, \tag{34}$$

$$s_\mathrm{g} = 1 - s_\mathrm{l}. \tag{35}$$

2.4. Boundary conditions

Oxygen is consumed at the catalyst layer, and its flux is related to the local current density by

$$N_{O_2} = \frac{M_{O_2}}{4F} I. \tag{36}$$

The local current density depends on various physical and chemical parameters of the catalyst layer, such as catalyst loading, porosity, catalyst layer width, oxygen concentration, overpotential and proton conductivity. The electrochemical reaction in the catalyst layer is modeled by a pseudo-homogeneous model, which is described in detail in [13].

Water is produced in the catalyst layer and water may also transport through the membrane under three different transport mechanisms:

1. electro-osmotic drag;
2. back diffusion by the water concentration difference between two sides of the membrane;
3. hydraulic permeation by pressure gradient between the cathode side and the anode side.

In general, the net water transport through the membrane can be represented as the net water molecules per proton [3,14] or net water transport coefficient

$$\alpha = n_d - D_w \frac{F}{I} \frac{dC_w}{dy} - C_w \frac{K_m}{\mu} \frac{F}{I} \frac{dp_w}{dy} \tag{37}$$

or

$$\alpha = n_d - n_{diff} - n_{hyd}, \tag{38}$$

where

$$n_d = 2.5 \frac{\lambda}{22}, \tag{39}$$

$$n_{diff} = D_w \frac{F}{I} \frac{dC_w}{dy}, \tag{40}$$

$$n_{hyd} = C_w \frac{K_m}{\mu} \frac{F}{I} \frac{dP_w}{dy}. \tag{41}$$

According to the above definitions, α can be positive or negative depending on the magnitudes of the three different water transport coefficients. A positive α indicates net water transport from anode side to cathode side. The water transport flux leaving the catalyst layer through the gas diffuser is the sum of the water generated in the cathode catalyst layer and the net water crossing over to the cathode from the anode.

$$N_w = -\frac{M_w(1+2\alpha)}{2F} I. \tag{42}$$

The mixture vertical velocity at the gas diffuser/catalyst layer interface is

$$\varepsilon v\Big|_{y=d_1+d_2} = \frac{(N_{O_2} + N_w)}{\rho}\Big|_{y=d_1+d_2}. \tag{43}$$

The axial velocity at the gas diffuser/catalyst layer interface is assumed to be zero according to no-slip boundary condition, thus the pressure gradient can be simplified by Darcy's law

$$\frac{dP}{dy} = -\frac{\mu}{K} v. \tag{44}$$

If natural convection is neglected, the oxygen and water concentration gradient can be obtained as

$$-D \frac{\partial(\rho C)}{\partial y} = N - \gamma_\alpha \rho \varepsilon v C. \tag{45}$$

Details on other boundary conditions and numerical procedures are discussed in [15] and will not be provided here due to space limitations.

3. Results and discussions

3.1. Validation of mathematical model

By solving the continuity, momentum and the species conservation equations in the cathode and anode sides, along with the governing equations in the catalyst layer and membrane, the performances of PEM fuel cell can be predicted. Table 1 lists the main geometric and operating parameters for the base case.

Rigorous numerical tests were performed to ensure that the solution of the simulation is independent of the grid size. The grid size tests show that the grid number of

Table 1
The base case parameters in the model

Channel length (cm)	7.0
Channel width (cm)	0.1
Gas diffuser width (cm)	0.03
Catalyst layer width (cm)	1.29×10^{-3}
Membrane width (cm)	1.08×10^{-2}
Gas diffuser porosity	0.4
Gas diffuser tortuosity	1.5
Catalyst layer porosity	0.25
Air stoic ratio	3.5
Hydrogen stoic ratio	2
Air humidification temperature (°C)	60
Hydrogen humidification temperature (°C)	60
Air pressure (Pa)	3.039×10^5
Hydrogen pressure (Pa)	1.013×10^5
Fuel cell temperature (°C)	80
Catalyst surface area (cm^2 cm^{-3})	1.4×10^5
Exchange current density (A/cm^2)	4.84×10^{-8}
Cathodic transfer coefficient	0.52
Anodic transfer coefficient	0.54
Dry membrane density (kg/m^3)	2.16
Ionomer equivalent weight	1100

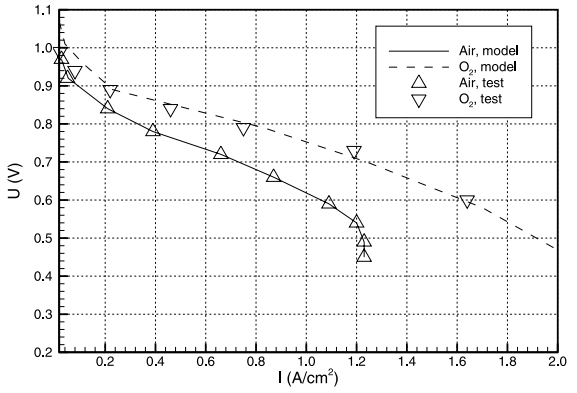

Fig. 2. The comparison of PEM fuel cell performance using air and oxygen, respectively. Air or O_2 side: $P_{in} = 3$ bar, $T_{hyd} = 60$ °C, $u_{in} = 0.35$ m/s; hydrogen side: $P_{in} = 1$ bar, $T_{hyd} = 60$ °C, $u_{in} = 0.6$ m/s; fuel cell operating temperature $T_{cell} = 80$ °C.

140×60 provides satisfactory results, and it was used in the simulations in this work.

To validate the model, polarization curves predicted by the model for air and oxygen are compared with experimental results, as shown in Fig. 2. It can be seen that reasonable agreements are obtained.

3.2. Two-dimensional species field

In the cathode catalyst layer, oxygen is consumed and water is produced. The water flux through the membrane depends on the combined actions of water hydraulic permeation, back diffusion and the electro-osmotic action. Water may flow from the anode side to the cathode side or from the cathode side to the anode side.

Fig. 3 shows the cathode-side oxygen and water-mass fraction in the "two-phase mixture", respectively, when the overall fuel cell current density is 1.07 A/cm^2. It should be noted that the thickness of the catalyst layer in these figures is enlarged 10 times for a clearer illustration. The oxygen fraction decreases along the flow direction due to oxygen consumption in the catalyst layer; water fraction increases due to water production in the cathode catalyst layer and the transport of water from the anode side. Considering the enlarged scale for the catalyst layer, it is obvious that the oxygen-mass fraction gradient in the catalyst layer is much higher than those in the gas diffuser and gas channel.

It is shown in Fig. 3(b) that the water mass fraction near the channel outlet is relatively high, where the corresponding water partial pressure is higher than the saturated vapor pressure at local temperature, indicating the formation of liquid water. Fig. 4(a) shows the water vapor mass fraction in the "gas phase" mixture. Because the air humidification temperature is less than the fuel cell operation temperature, the inlet air is unsaturated. The vapor mass fraction increases along the channel due to the evaporation of liquid water from the catalyst layer. When the air reaches saturation state, liquid water is formed. The saturation line may be called the "condensation front." Fig. 4(a) shows that the water vapor fraction increases at the inlet of the channel and becomes constant after the condensation front.

Fig. 4(b) shows the corresponding liquid water saturation field. The liquid saturation is zero in the single-phase region. Inside the two-phase region, the liquid saturation increases along the flow direction. The liquid saturation decreases from the catalyst layer toward the gas channel due to water transport from the catalyst layer. Fig. 5 shows the liquid phase velocity vector in the cathode gas diffuser. The liquid velocity vector points to the gas channel/gas diffuser interface, so the liquid water is carried away from the gas diffuser, and the liquid saturation in the gas channel increases.

Fig. 6 displays the corresponding variation of various water transport coefficients along the flow direction for

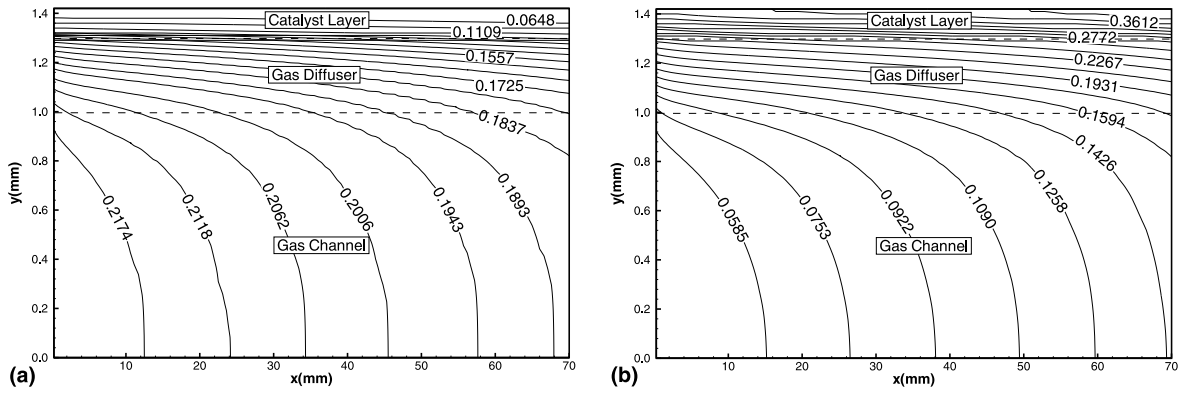

Fig. 3. Oxygen and water mass fraction in the "two-phase" mixture in the cathode gas channel, gas diffuser and catalyst layer: (a) oxygen; (b) water.

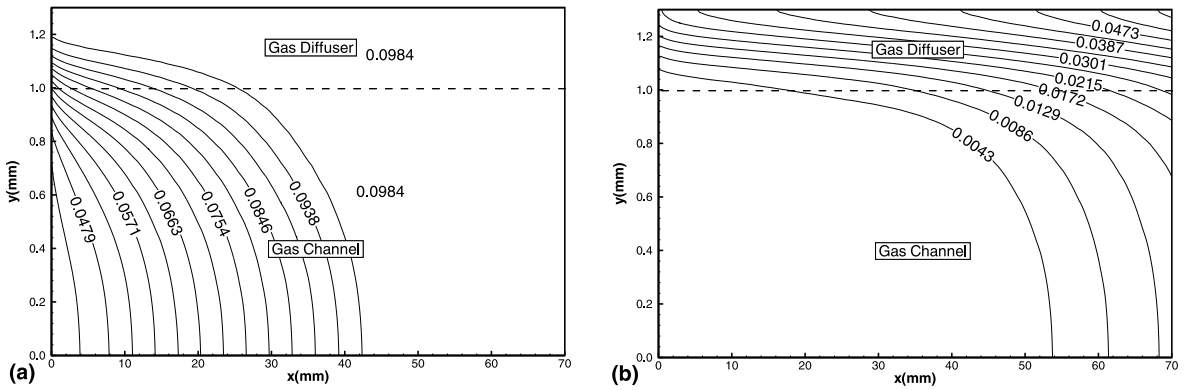

Fig. 4. Water vapor mass fraction in the gas phase mixture and the liquid saturation field in the cathode gas channel and the gas diffuser: (a) water vapor mass fraction; (b) liquid saturation.

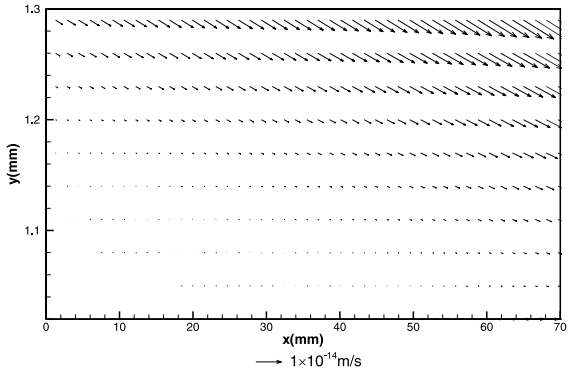

Fig. 5. Liquid water velocity vector in the cathode gas diffuser.

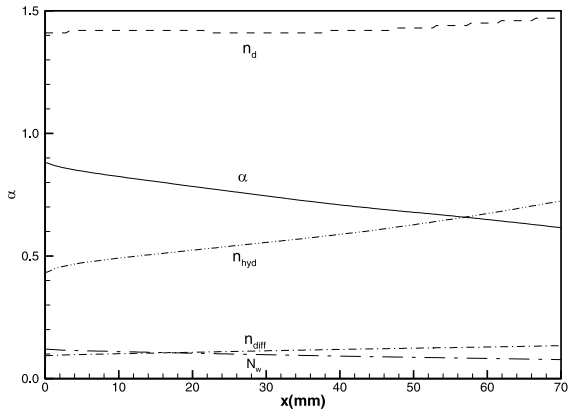

Fig. 6. The electro-osmotic, net, diffusion and hydraulic permeation water transport coefficient across the membrane along the flow direction.

the base case. When water concentration in the cathode side is higher than that in the anode side, there is a diffusion water flux from the cathode side to the anode side. It is often called "back-diffusion", because it is in the opposite direction to the water transfer due to electro-osmotic drag. In the flow direction, the water activity increases in the cathode side and decreases in the anode side, resulting in the diffusion water flux from the cathode side to the anode side to increase. For the case studied here, the cathode gas pressure and anode gas pressures are 3 and 1 bar, respectively, the resulting pressure difference causes water permeation flux from the cathode side to the anode side. With the water production in the cathode side and water transfer from the anode side, the water partial pressure difference between the cathode side and the anode side increases, which causes an increase in n_{hyd} in the flow direction too. Another reason for the increase of n_{diff} and n_{hyd} is that they are inversely proportional to the local current density according to Eqs. (40) and (41). As the current density decreases along the flow direction, the values of n_{diff} and n_{hyd} are higher even though the corresponding water flux is the same. The electro-osmotic coefficient depends on the water content and the physical properties of the membrane. The electro-osmotic coefficient increases slightly along the flow direction because of the increase of water content in the membrane. Combining the above three water transport mechanisms, the net water transport coefficient is depicted as a solid line in Fig. 6. The net water transport coefficient decreases along the flow direction, reflecting the increasing effects of back diffusion and hydraulic permeation. Since the water flux is proportional to the net water transport coefficient and the local current density, the net water flux decreases along the flow direction.

3.3. The effect of operating current density on the liquid saturation

As discussed above, for most PEM fuel cell operating conditions, especially under a high current density,

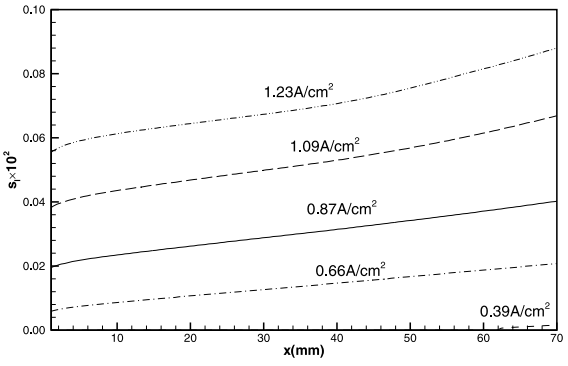

Fig. 7. The liquid saturation at the gas diffuser/catalyst layer interface under different current densities for the base case.

water is transported from the anode to the cathode side. In addition, water is produced at the cathode catalyst layer, resulting in the water mass fraction being highest at the gas diffuser/catalyst layer interface, which is also the most likely place where liquid water forms. Therefore, the liquid saturation at the gas diffuser/catalyst layer interface is an indication of the existence of two-phase flow and the amount of liquid phase in the gas diffuser. Fig. 7 shows the liquid saturation distribution at the gas diffuser/catalyst layer interface under different current densities for the base case. For any specific current density, liquid saturation increases along the flow direction, reflecting the effect of water accumulation. The magnitude of liquid saturation also increases with the current density. When the fuel cell operates under a low current density, no liquid water is formed in the cathode. While the current density increases to $I = 0.39$ A/cm^2, liquid water is formed beginning from $x = 62$ mm, and the liquid saturation is very low. With further increase of the current density, the two-phase region extends to the beginning of the flow passage.

3.4. The effect of fuel cell operating temperature

The operating temperature is an important parameter for PEM fuel cell performance. At a low temperature, oxygen reduction needs higher activation overpotential to produce the same current density. On the other hand, the membrane resistance is lower at a low temperature than at a high temperature, because water activity is higher at a low temperature for the same water content. Thus, there exists an optimum operation temperature for PEM fuel cells. Operating temperature also influences the two-phase flow in the cathode. At a low temperature, liquid water is more likely to form. It can be seen in Fig. 7 that the liquid saturation at point F (Fig. 1) is the highest in the gas diffuser, thus point F can represent the occurrence of the two-phase flow in the gas diffuser. When the liquid saturation at point F is positive, two-phase flow initiates. Fig. 8(a) shows the variation of the liquid saturation at point F with the current density for different operating temperatures. When the fuel cell operates at a temperature 60 °C, liquid water is formed at very small current density. When the operating temperature increases, the threshold current density to form liquid water in the gas diffuser also increases. The threshold current density is about 0.79 A/cm^2 for operating temperatures at 90 °C. No liquid water is formed when the fuel cell operating temperature is 100 °C. This conclusion agrees with our expectation that at the same current density liquid saturation tends to be higher at lower temperatures than at higher temperatures.

For the same reason, point C in Fig. 1, where liquid water is the most likely to form in the channel, can be used to determine the existence of two-phase flow in the channel. Fig. 8(b) shows the variation of the liquid saturation at point C with the current density for different fuel cell operating temperatures. Because the liquid saturation at point C is lower than that at point F

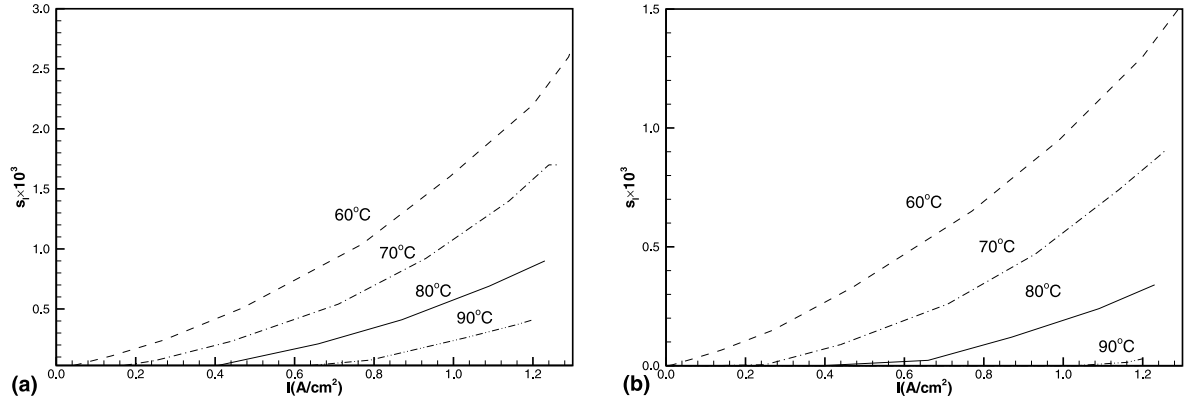

Fig. 8. The variation of liquid saturation with current density for different fuel cell temperatures: (a) point F in Fig. 1; (b) point C in Fig. 1.

under the same current density, this proves that the two-phase flow is first formed in the gas diffuser. In the gas channel, the threshold current density needed to form liquid water is also generally higher than in the gas diffuser. With an operating temperature of 90 °C, the threshold current density is as high as 1.1 A/cm^2 in the gas channel, compared with that of 0.79 A/cm^2 in the gas diffuser. No liquid water is formed in the gas channel at all when the operating temperature is 100 °C.

3.5. The effect of air humidification temperature

To ensure certain membrane humidification, air is usually humidified in the cathode side in a PEM fuel cell operation. Humidifying air stream can increase the water concentration gradient between the cathode and the anode sides and increase the water back diffusion flux and hydraulic permeation flux from the cathode side to the anode side, thus keeping the membrane batter hydrated. However, due to the increased water content in the cathode, it is easier to form two-phase flow in the gas diffuser, especially at a high humidification temperature. A high air humidification temperature also decreases the oxygen partial pressure, which increases the concentration overpotential and reduces the cathode limiting current density. Fig. 9 shows the variation of liquid saturation at points F and C with the current density for different air humidification temperatures. Similar to the different operating temperature, the liquid saturation in both the gas diffuser and the gas channel increases with the operating current density. When the air humidification temperature is less than or equal to the fuel cell operating temperature, the threshold current density needed to form liquid water in the gas diffuser is higher than that in the gas channel. The liquid saturation in the gas diffuser (point F) is also higher than that in the gas channel (point C), which means liquid water flows toward the gas channel. However, while the inlet air humidification temperature (e.g., 100 °C) is higher than the fuel cell operating temperature (e.g., 80 °C) and the fuel cell is operated at a low current density (< 0.33 A/cm^2), the liquid saturation in the gas channel (point C) is higher than that in the gas diffuser (F point). Thus, the liquid water flows from the cathode side to the anode side. Two-phase flow is formed from the beginning of the flow channel and exists in the whole channel even at $I = 0$.

It should also be noted that the maximum current densities in Fig. 9 are different for different air humidification temperatures, which reflects the fact that liquid water caused by a high air humidification temperature does reduce the limiting current density.

3.6. The effect of anode humidification temperature

Because the water tends to flow from the anode side to the cathode side under the electro-osmotic drag in the membrane, the humidification of anode gas is the most effective and most common method to humidify the membrane. If insufficient water is provided in the anode side, the membrane is prone to dehydration. Sufficient water is favorable to decrease the membrane proton resistance, but too much water increases the possibility of forming liquid water in the cathode gas diffuser and decreases the oxygen mass fraction and the cathode limiting current density. In addition, high anode humidification temperature decreases the hydrogen partial pressure, thus the anode limiting current density decreases too. This may have no significant effect when pure hydrogen is used, but the effect becomes more pronounced when reformed gas is used where N_2 and CO_2 represent substantial fractions. Fig. 10 shows the variation of liquid saturation at points F and C in the cathode side with the current density for different anode humidification temperatures. Similar to the discussions before, the liquid saturation in both the gas diffuser and in the gas channel increases with the operating current

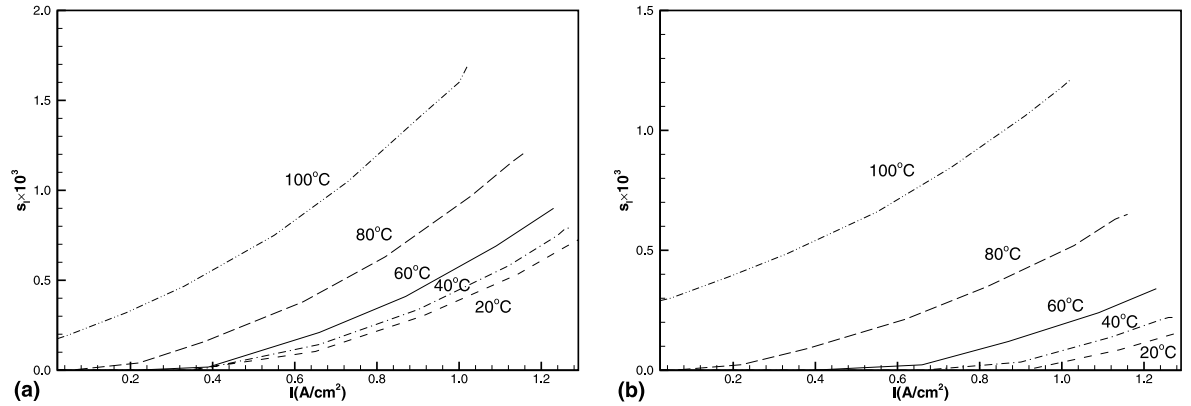

Fig. 9. The variation of liquid saturation with current density for different air inlet humidification temperatures: (a) point F in Fig. 1; (b) point C in Fig. 1.

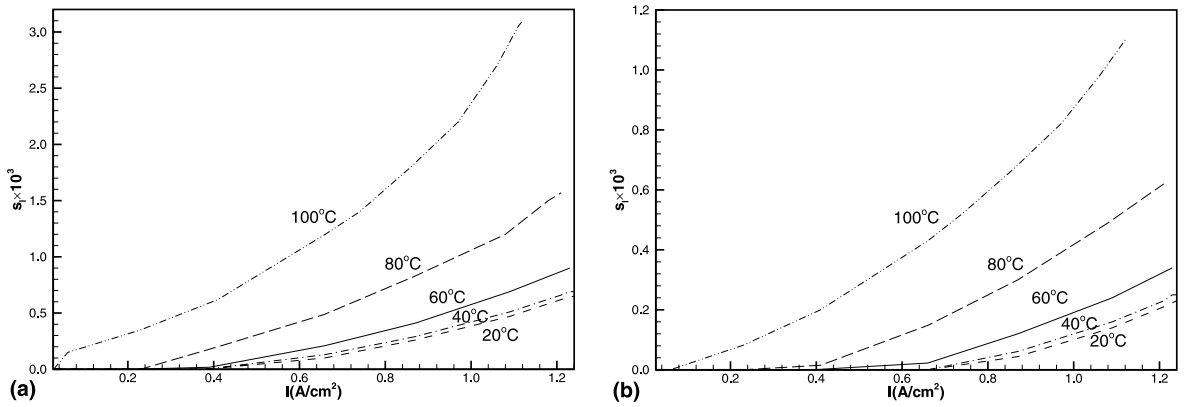

Fig. 10. The variation of liquid saturation with current density for different hydrogen inlet humidification temperatures: (a) point F in Fig. 1; (b) point C in Fig. 1.

density, and the liquid saturation at F is higher than that at C. When the anode humidification temperature is 100 °C, the magnitude of liquid saturation in the gas diffuser is even higher than that at air humidification temperature at 100 °C, which means that anode humidification is an important factor to form liquid water in the cathode side. At high anode humidification temperature (e.g., 100 °C), the liquid water is formed in the gas diffuser and in the fluid channel when the fuel cell is operated at a very low current density. With the anode humidification temperature decreasing, the threshold current densities for both the gas diffuser and the cathode gas channel increase. The threshold current densities in the cathode gas diffuser and in the cathode gas channel are about 0.66 and 0.87 A/cm^2, respectively, when the hydrogen humidification temperature is 20 °C. We may also observe that the limiting current density decrease to about 1.12 A/cm^2 when the hydrogen humidification temperature is 100 °C.

Besides the factors discussed above, the characteristics of the porous media, such as porosity, permeability and surface tension coefficients, definitely affect the two-phase flow characteristics, which will be studied in future work.

4. Conclusions

A two-dimensional, two-phase and multi-component model has been developed to model the flow and transport in the combined gas channel and porous gas diffuser in the PEM fuel cell. The model does not need to assume the "condensation front" as a *priori*; it may predict the formation and distribution of two-phase flow in the gas diffuser and the gas channel simultaneously. The following conclusions can be derived from this study:

1. The net water transport coefficient depends on the operating current density, the water activity on the cathode and anode sides, the water partial pressure on two sides, and the membrane properties.
2. The threshold current density needed to form two-phase flow and the distribution of liquid saturation in the cathode side depends on the fuel cell operating temperature, cathode and anode humidification temperatures and the characteristics of porous gas diffuser.
3. The two-phase flow model provides a more realistic simulation in the flow and transport in the PEM fuel cell. It could be a very valuable tool for water and thermal management, as well as for the design and operation of PEM fuel cells.

Acknowledgements

The financial support of the US Department of Energy's CARAT program under contract DE-FC02-98EE50531 is gratefully acknowledged.

References

[1] D.M. Bernardi, M.W. Verbrugge, Mathematical model of a gas diffusion electrode bonded to a polymer electrolyte, AIChE J. 37 (1991) 1151–1163.
[2] D.M. Bernardi, M.W. Verbrugge, A mathematical model for the solid-polymer-electrode fuel cell, J. Electrochem. Soc. 139 (1992) 2477–2491.
[3] F.E. Springer, T.A. Zawodzinski, S. Gottesfeld, Polymer electrolyte fuel cell model, J. Electrochem. Soc. 138 (1991) 2334–2342.
[4] T.F. Fuller, J. Newman, Water and thermal management in solid-polymer-electrolyte fuel cells, J. Electrochem. Soc. 140 (1993) 1218–1225.

[5] T.V. Nguyen, R.E. White, A water and thermal management model for proton-exchange-membrane fuel cells, J. Electrochem. Soc. 140 (1993) 2178–2186.
[6] V. Gurau, H.T. Liu, S. Kakac, Two-dimensional model for proton exchange membrane fuel cells, AIChE J. 44 (1998) 2410–2422.
[7] Z.H. Wang, C.Y. Wang, K.S. Chen, Two-phase flow and transport in the air cathode of PEM fuel cells, J. Power Source 94 (2001) 40–50.
[8] C.Y. Wang, P. Cheng, A multiphase mixture model for multiphase, multi-component transport in capillary porous media – I: model development, Int. J. Heat Mass Transfer 39 (1996) 3607–3618.
[9] L.M. Abriola, G.F. Pinder, A multiphase approach to the modeling of porous media contamination by organic compounds I. Equation development, II. Numerical simulation, Water Resour. Res. 21 (1985) 11–26.
[10] K. Vafai, C.L. Tien, Boundary and inertia effects on flow and heat transfer in porous media, Int. J. Heat Mass Transfer 24 (1981) 195–203.
[11] M. Kaviany, Principles of Heat Transfer in Porous Media, Springer, New York, 1995.
[12] M.C. Leverett, Capillary behavior in porous solids, Trans. AIME 142 (1941) 152–169.
[13] L. You, H.T. Liu, A parametric study of the cathode catalyst layer of PEM fuel cells using a pseudo-homogeneous model, Int. J. Hydrogen Energy 26 (2001) 991–999.
[14] J.S. Yi, T.V. Nguyen, An along-the-channel model for PEM fuel cells, J. Electrochem. Soc. 145 (1998) 1149–1159.
[15] L. You, The two-phase flow, transport mechanism and performance studies for PEM fuel cells, Ph.D. Dissertation, University of Miami, Miami, FL, 2001.